

BaFe₂Se₂O as an Iron-Based Mott Insulator with Antiferromagnetic Order

Fei Han^{1,2}, Xiangang Wan¹, Bing Shen^{1,2}, and Hai-Hu Wen^{1*}

¹Center for Superconducting Physics and Materials,
National Laboratory of Solid State Microstructures and Department
of Physics, Nanjing University, Nanjing 210093, China and

²National Laboratory for Superconductivity, Institute of Physics
and Beijing National Laboratory for Condensed Matter Physics,
Chinese Academy of Sciences, Beijing 100190, China

A iron-based compound with a quasi-two-dimensional array of FeSe₃O tetrahedra and an orthorhombic structure, namely BaFe₂Se₂O, has been successfully fabricated. Experimental results show that this compound is an insulator and has an antiferromagnetic (AF) transition at 240 K. Band structure calculation reveals the narrowing of Fe 3d bands near the Fermi energy, which leads to the localization of magnetism and the Mott insulating behavior. The large distances between the Fe atoms perhaps are responsible for the characters. Linear response calculation further indicates a strong in-plane AF exchange J , this can account for the enhanced magnetic susceptibility (which has a maximum at about 450 K) above the Neel temperature.

PACS numbers: 71.10.Hf, 71.27.+a, 71.55.-i, 75.20.Hr

A. Introduction

Discovery of the copper-based superconductors¹ with high transition temperatures (T_c) has attracted great attention and triggered extensive research in the fields of condensed matter physics and material sciences. High- T_c superconductivity in the cuprates occurs with either hole or electron doping in the antiferromagnetic (AF) Mott insulating parent compounds. The Mottness clearly plays an important role here². In the past years, scientists have been trying to explore new high- T_c superconductors in non-copper-based compounds. Until four years ago, the discovery of superconductivity at 26 K in oxy-arsenide LaFeAsO_{1-x}F_x³ broke the uniqueness of cuprates in giving rise to high- T_c superconductivity. This is actually a surprise since Fe atoms are normally strongly magnetic in materials and usually inhibit superconductivity. Among the iron-based superconductors with several different structures³⁻¹¹, it is widely perceived that the common FeX ($X =$ pnictide or chalcogenide) layers are responsible for the superconductivity. Meanwhile, for many FeAs-based superconductors, their parent phases possess an AF order which seems to compete with the superconductivity. To unravel the mystery of the origin of magnetism and its relation with superconductivity is the most important issue. Now there exist two major pictures, namely the electron pairing is established through a weak coupling by exchanging the AF spin fluctuations^{12,13}, or the pairing is furnished by the local strong pairing^{14,15}. Related to this debate, it has been argued whether the magnetism in the iron-based superconductors is localized or itinerant in nature. It thus becomes very important to find a iron-based compound with a formally known knowledge of localized or itinerant magnetism. Recently, exploration along this line was successful in finding the materials of $Re_2O_2Fe_2O(Se/S)_2$ ^{16,17} ($Re =$ rare earth element), La₂Co₂Se₂O₃¹⁸, La₂O₃Mn₂Se₂¹⁹ and Na₂Fe₂Se₂O²⁰. These compounds all contain an ex-

panded similar square-planar M lattice in their M_2OSe_2 ($M =$ Fe, Co and Mn) layers. Here we report the fabrication of an iron-based compound BaFe₂Se₂O. From the structure point of view, it looks like the existing materials $Re_2O_2M_2O(Se/S)_2$ and Na₂Fe₂Se₂O. However, a closer scrutiny finds the clear difference between them, since the compound BaFe₂Se₂O contains a honeycomb-like Fe sublattice instead of the square-planar Fe lattice. The compound has an orthorhombic structure and is revealed to be a Mott insulator with a localized antiferromagnetism.

B. Experimental Details

The single-crystalline sample was synthesized with the starting materials BaO and FeSe in the ratio of 1:2 by using a flux method, similar to a previous synthesis of $K_xFe_{2-y}Se_2$ ²¹. The resultant crystals were black shining platelets with a typical dimension of $1.5 \times 1.5 \times 0.5$ mm³. To determine the compositional ratio of atoms in the compound, scanning electron microscope and energy-dispersive x-ray spectroscopy (EDX) measurements were carried out on the crystals. Powder X-ray diffraction (XRD) pattern was measured on the smashed and powdered crystals with $\theta - 2\theta$ scan at room temperature. The XRD data were analyzed by a Rietveld method with the software GSAS²². Resistivity measurement was done using a four-probe technique on the physical property measurement system (PPMS). Dc magnetic susceptibility was measured on a superconducting quantum interference device (SQUID). Specific heat was also measured using a relaxation technique on the PPMS.

C. Experimental Data and Discussion

1. Crystal Structure

The energy-dispersive x-ray spectroscopy (EDX) of the crystals is shown in Fig. 1(a). One can see that the crystals are composed of Ba, Fe, Se and O elements. The ratio of atoms is determined as Ba:Fe:Se = 20.61:39.94:39.45 (close to 1:2:2) while the amounts of O can not be quantified accurately. The EDX result offers us a basis for seeking suitable reference compound to do phase identification. We finalize our compound isostructural to β -BaFe₂S₃ (formerly reported as Ba₂Fe₄S₅^{23,24}). β -BaFe₂S₃ may be viewed as an average due to twinning of a polymorph of α -BaFe₂S₃ which contains iron-deficient-FeAs-layers-like Fe₂S₃ layers^{25–27}. BaFe₂Se₂O can be considered as a derivative of β -BaFe₂S₃ by replacing the S atoms at 2b sites with O atoms and the S atoms at 4e sites with Se atoms. The powder x-ray diffraction (XRD) pattern and Rietveld fit for the smashed and powdered crystals is shown in Fig. 1(b). The data is well fitted with an orthorhombic BaFe₂Se₂O phase which has the space group of *Pmnm*. The unit cell is given in the inset of Fig. 1(b). The starting parameters for the fit are taken from β -BaFe₂S₃²⁴ and the GSAS program finally finds the best fitting parameters. In Table I, the best fitting structure parameters are listed. As shown in Fig. 1(c), in BaFe₂Se₂O, the nearest neighbor atoms of each Fe atom, namely the three Se atoms and one O atom, surround the Fe atom and form a tetrahedra. The structure of BaFe₂Se₂O can also be viewed as an infinite quasi-two-dimensional array of FeSe₃O tetrahedra. Upper and lower Fe ladders along the *a* direction and zig-zag Fe chains along the *b* direction forms uneven Fe layers. Obviously, there is not a strictly speaking square-planar Fe lattice in this compound. It is interesting to notice that the upper and lower Fe ladders form a non-coplanar honeycomb-like structure, as shown in Fig. 1(d).

2. Transport properties

Fig. 2 gives the resistivity measurement result for the BaFe₂Se₂O single-crystalline sample. The room-temperature resistivity measured is as high as 100 Ω cm which is comparable to those of La₂O₂Fe₂OSe₂¹⁶, Na₂Fe₂Se₂O²⁰ and Ba₂F₂Fe₂OSe₂²⁸. In the temperature dependence of resistivity, an insulating behavior is observed, and the resistivity divergence in the low temperature region below 150 K can be fitted by the model of variable-range-hopping: $\rho(T) = \rho_0 \exp(T_0/T)^{\frac{1}{4}}$. This result was also observed in many 3d transition metal compounds in which the correlation is assume to be strong.

The temperature dependence of dc magnetic susceptibility for the BaFe₂Se₂O single-crystalline sample is presented in Fig. 3(a). The dc magnetic susceptibility measurement was carried out under a magnetic field of 20000 Oe in zero-field cooling (ZFC) process. We can see

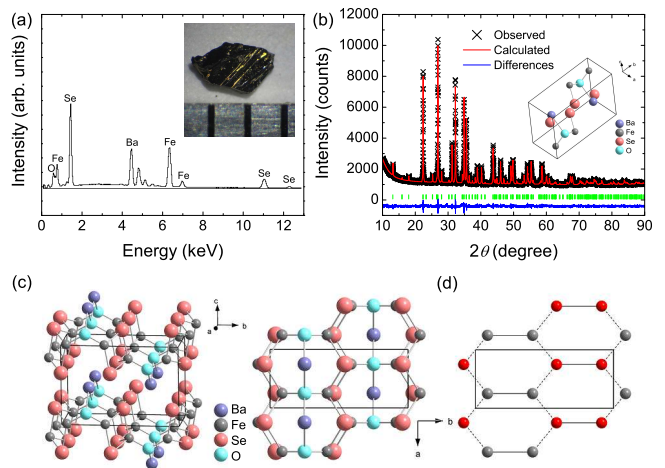


FIG. 1: (Color online) (a) Energy-dispersive x-ray spectroscopy (EDX) of the crystal. The inset shows a crystal with the typical dimension of $1.5 \times 1.5 \times 0.5$ mm³. (b) Powder X-ray powder diffraction (XRD) pattern and Rietveld fit for the smashed and powdered crystals. The inset shows a unit cell of BaFe₂Se₂O. (c) Crystal Structure of BaFe₂Se₂O. (d) Honeycomb-like Fe sub-lattice in BaFe₂Se₂O, the gray balls and the red balls all indicate Fe atoms, with the gray balls forming the upper ladder and the red balls forming the lower ladder, respectively.

TABLE I: Crystallographic data of BaFe₂Se₂O.

Space group	<i>Pmnm</i>
<i>a</i> (Å), <i>b</i> (Å), <i>c</i> (Å)	4.14028(5), 9.86716(14), 6.73381(8)
<i>V</i> (Å ³)	275.095
<i>Z</i>	2
<i>R_p</i> , <i>wR_p</i>	2.41%, 3.12%
Atomic parameters:	
Ba	2a ($\frac{1}{4}$, $\frac{1}{4}$, <i>z</i>) <i>z</i> =0.50850(18)
Fe	4e ($\frac{1}{4}$, <i>y</i> , <i>z</i>) <i>y</i> =0.91347(22), <i>z</i> =0.87920(27)
Se	4e ($\frac{1}{4}$, <i>y</i> , <i>z</i>) <i>y</i> =0.95840(15), <i>z</i> =0.24251(20)
O	2b ($\frac{1}{4}$, $\frac{3}{4}$, <i>z</i>) <i>z</i> =0.7502(13)
Bonding lengths (Å):	
Ba-O	2.706(6)×2
Fe-O	1.832(4)×1
Fe-Se	2.5604(15)×2
Fe-Se	2.4863(23)×1
Fe-Fe	3.1382(13)×2
Fe-Fe	3.2260(12)×1
Bonding angles (degree):	
Se-Fe-Se	103.11(6)×2
Se-Fe-Se	107.90(9)×1
Se-Fe-O	106.44(14)×2
Se-Fe-O	128.57(29)×1

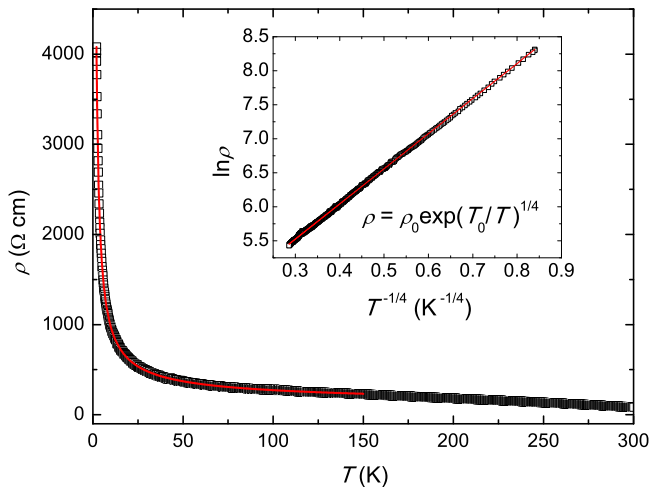


FIG. 2: (Color online) Temperature dependence of resistivity for the BaFe₂Se₂O single-crystalline sample. The inset shows that $\ln \rho$ is directly proportional to $T^{-1/4}$ below 150 K.

a kink associated with the AF transition at about 240 K in the $\chi(T)$ curve. This transition is indicated more clearly by the peak in the $d(\chi T)/dT$ versus T curve, as shown in the inset of Fig. 3(a). Similar AF transition is observed in the parent compounds of cuprates and some iron-based superconductors^{29–31}. Above 240 K, the magnetic susceptibility exhibits a continuing enhancement, which is observed in many two-dimensional magnetic systems including the parent compounds of iron-based superconductors^{30,31} and is explained as due to the short-range correlation of the local moments³². The continuing enhancement leads to a broad maximum around $T_{max} = 450$ K. The ratio of T_N/T_{max} is usually used to estimate the extent of the low-dimensional magnetic correlations. As T_N/T_{max} in our BaFe₂Se₂O is 0.53, it can be concluded that BaFe₂Se₂O is a quasi-two-dimensional magnetic system.

In order to further understand the magnetic transition, we performed a specific heat measurement, as shown in Fig. 3(b). Provided the negligible contribution by the magnons at very low temperatures ($T \ll T_N$), the specific heat can be separated into electronic and phonon parts: $C(T) = \gamma T + \beta T^3$. We find that the low temperature data show no electronic contribution, consistent with the insulating ground state. From the slope (β) of the straight line in the C/T vs T^2 plot (as shown in the inset of Fig. 3(b)), we obtain the Debye temperature $\Theta_D = 224.5$ K using the formula $\Theta_D = [12\pi^4 N R / (5\beta)]^{1/3}$, where N is the number of atoms in the chemical formula and R refers to the ideal gas constant $8.314 \text{ J mol}^{-1} \text{ K}^{-1}$. Since the Debye model fails to reproduce the $C(T)$ data at high temperatures, we employ a polynomial to fit the phonon contribution in the temperature range from 50 to 300 K. Assuming that the total specific heat consists of phonon and magnetic components, the magnetic contribution can be obtained simply by the subtraction of the

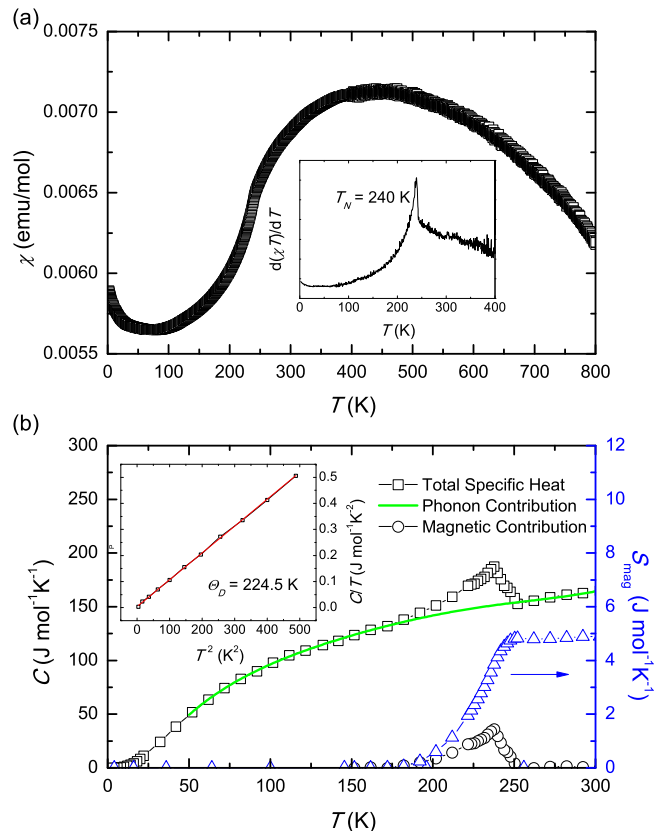


FIG. 3: (Color online) (a) Temperature dependence of dc magnetic susceptibility for the BaFe₂Se₂O single-crystalline sample in zero-field-cooling (ZFC) process at a magnetic field of $H = 20000$ Oe. The inset shows the $d(\chi T)/dT$ versus T curve. We can see a peak associated with an AF transition at 240 K. (b) Temperature dependence of specific heat for the BaFe₂Se₂O single-crystalline sample. The green solid curve represents the phonon contribution, fitted by a polynomial. After deducting the phonon contribution, the specific heat contributed by magnetic shows a peak at 240 K. Part of the magnetic entropy has been dissipated above 240 K.

phonon contribution. A heat-capacity peak appears at 240 K which is exactly the temperature where the magnetic susceptibility exhibits a sharp step (as illustrated by the derivative $d(\chi T)/dT$). The magnetic entropy can be calculated using the integral $S_{mag} = \int_0^T C_{mag}/T dT$. The result gives $S_{mag} = 4.89 \text{ J mol}^{-1} \text{ K}^{-1}$. Part of the magnetic entropy has been dissipated above 240 K. Although the AF occurs at about 240 K, as reflected from the $d(\chi T)/dT$ data, we find a significant contribution of entropy due to the strong AF fluctuation above 240 K.

D. Band Structure Calculations

To have a comprehensive understanding on the physical properties of BaFe₂Se₂O, we also perform the density-functional theory calculations based on the local density approximation (LDA) to density functional theory with

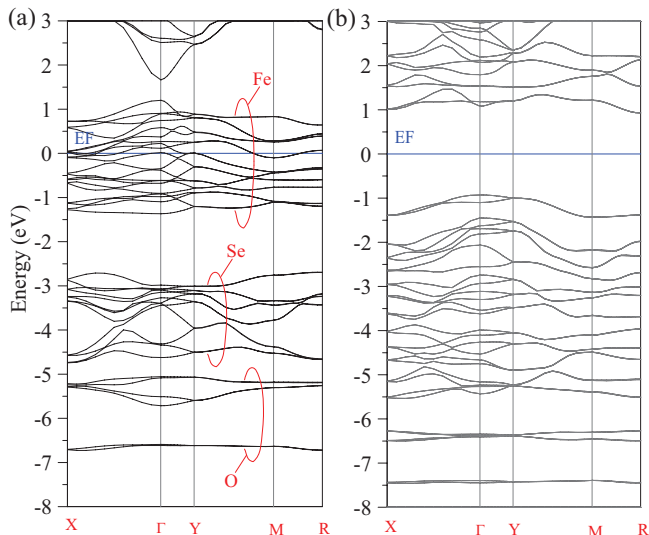


FIG. 4: Band structure from LDA calculation, and LDA+ U calculation with $U = 6.0$ eV.

the full-potential, all-electron, linear-muffin-tin-orbital method³³. To see the basic features of the electronic structure, we first do nonmagnetic LDA calculation, and show the band structure in Fig. 4a. Although with strong hybridization, the Fe, Se and O bands are separated as shown in Fig. 4a. The six bands located from -6.6 to -5.0 eV basically come from O 2*p* states, the twelve bands located from -5.0 to -3.4 eV are mainly contributed by Se 4*p* states, while the twenty Fe 3*d* bands distribute from -1.4 to 1.2 eV. The non-coplanar honeycomb-like structure significantly narrows the band, consequently, the bandwidth of Fe 3*d*, Se 4*p* and O 2*p* bands are considerably narrower than these of Fe-based superconductor and $\text{La}_2\text{O}_2\text{Fe}_2\text{OSe}_2$ ¹⁶.

We then perform the spin polarized calculation. We first evaluate the interlayer magnetic exchange interaction based on our linear response scheme³⁴. Our numerical results show that similar with Fe-based superconductor³⁵, the exchange process happens almost completely in the Fe-Se-O layer, and the inter-layer exchange interaction is negligible. This result is consistent with the observed two-dimensional magnetic behavior. To search the ground state magnetic ordering configuration, we consider four spin alignments within layer as following: FM, AFM-1 (Fe1 and Fe2, Fe3 and Fe4 couple ferromagnetically while Fe2 and Fe3 have opposite spin orientation), AFM-2 (Fe1 and Fe2, Fe3 and Fe4 couple antiferromagnetically while Fe2 and Fe3 have the same spin orientation), AFM-3 (Fe atom couples with all of three nearest neighbor Fe antiferromagnetically). The three kinds of AFM spin alignments are plotted in Fig. 5. The LSDA calculation predicts that the AFM-3 has the lowest total energy, and the magnetic moment mainly locates at Fe site. It is interesting to notice that the calculated magnetic moment (about $3.0 \mu_B$) is not sensitive to the magnetic configuration. While for iron arsenides,

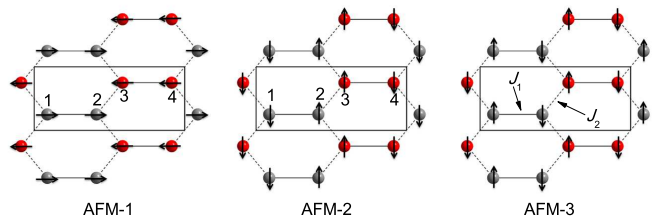


FIG. 5: Three kinds of possible AFM spin alignments within layer. AFM-3 has the lowest total energy.

the magnetism is quite itinerant and the magnetic moment strongly dependent on the magnetic configuration. Although can explain the AFM behavior, LSDA calculation fails to reproduce the observed insulating behavior.

It is well known that the Coulomb interaction for 3*d* orbital is significant, and estimates for the values of U have been recently done yielding $U \approx 5.0$ eV in Fe-based superconductors³⁶. Although the accurate value of U is not known for $\text{BaFe}_2\text{Se}_2\text{O}$, with narrower bands we generally expect it is larger than that of Fe-based superconductor. We therefore utilize LDA+ U scheme³⁷, which is adequate for the magnetically ordered insulating ground states³⁸, and set $U = 6.0$ eV. Same with LSDA calculation, LDA+ U calculation also predicts AFM-3 as the ground state, and the obtained magnetic moment is not depending on the magnetic configuration. As shown in Fig.4b, electronic correlation significantly changes the band structure and results in a considerable effective gap (about 1.86 eV). Our linear response calculation³⁵ shows that the magnetic exchange interaction is short range and the magnetic coupling further than the second nearest neighbor is almost equal to zero. The magnetic exchange interactions between all of three nearest neighbor Fe-Fe are AFM sign, which is consistent with the total energy comparison. The strength of exchange coupling ($J_1 = 96$ meV and $J_2 = 31$ meV) is similar with that of LaFeAsO ^{35,39}, which may account for the fact of similar magnetic susceptibility above the Neel temperature. We also vary parameter U between 2 and 8 eV for Fe 3*d* electrons to see what effects the on-site Coulomb repulsion would bring to the electronic structure of $\text{BaFe}_2\text{Se}_2\text{O}$. Our numerical calculation confirm that U does not change the qualitative results: AFM-3 is the ground state, the magnetism is local in nature, and the Coulomb interaction is essential for opening the band gap. The real magnetic structure will be determined by neutron diffraction method, just like the case of $\text{Re}_2\text{O}_3\text{Fe}_2\text{Se}_2$ ^{17,40}.

E. Concluding Remarks

In summary, a iron-based compound $\text{BaFe}_2\text{Se}_2\text{O}$ was synthesized successfully. It has an orthorhombic structure with the space group of $Pmmn$. Strictly speaking, there is not a square-planar Fe lattice in it, instead, it

contains a honeycomb-like Fe sub-lattice. The model of variable-range-hopping is used to explain the resistivity divergence in the low temperature region. An AF ordering transition at 240 K is observed both from the dc magnetic susceptibility and specific heat. Band structure calculation reveals the narrowing of Fe 3*d* bands near the Fermi energy, which leads to the localization of magnetism and the Mott insulating behavior. The distances between the Fe atoms (3.1382(13) Å and 3.2260(12) Å) perhaps are responsible for the characters, since they are so large that the overlap between the 3*d*-orbitals becomes very small. Linear response calculation further indicates a strong in-plane AF exchange *J*, this can account for the enhanced magnetic susceptibility (which has a maximum at about 450 K) above the Neel temperature. Considering the fact that the Mottness and AF order are

commonly occurring in cuprates and the iron pnictides, it would be interesting to know whether it is possible to induce superconductivity by either chemical doping or applying high pressure in our present system. This investigation is underway.

F. Acknowledgments

We are grateful to Qimiao Si and Igor I. Mazin for helpful discussions. This work is supported by the Natural Science Foundation of China, the Ministry of Science and Technology of China (973 project: 2011CBA00102) and PAPD.

-
- * Electronic address: hhwen@nju.edu.cn
- ¹ J. G. Bednorz, and K. A. Muller, *Z. Phys. B* **64**, 189 (1986).
 - ² P. W. Anderson, *Science* **235**, 1196 (1987).
 - ³ Y. Kamihara, T. Watanabe, M. Hirano, and H. Hosono, *J. Am. Chem. Soc.* **130**, 3296 (2008).
 - ⁴ M. Rotter, M. Tegel, and D. Johrendt, *Phys. Rev. Lett.* **101**, 107006 (2008).
 - ⁵ K. Sasmal, B. Lv, B. Lorenz, A. M. Guloy, F. Chen, Y. Y. Xue, and C. W. Chu, *Phys. Rev. Lett.* **101**, 107007 (2008).
 - ⁶ X. C. Wang, Q. Q. Liu, Y. X. Lv, W. B. Gao, L. X. Yang, R. C. Yu, F. Y. Li, and C. Q. Jin, *Solid State Commun.* **148** 538 (2008).
 - ⁷ J. H. Tapp, Z. Tang, B. Lv, K. Sasmal, B. Lorenz, P. C. W. Chu, and A. M. Guloy, *Phys. Rev. B* **78**, 060505(R) (2008).
 - ⁸ F. C. Hsu, J. Y. Luo, K. W. Yeh, T. K. Chen, T. W. Huang, P. M. Wu, Y. C. Lee, Y. L. Huang, Y. Y. Chu, D. C. Yan, and M. K. Wu, *Proc. Natl. Acad. Sci.* **105**, 14262 (2008).
 - ⁹ T. Klimczuk, T. M. McQueen, A. J. Williams, Q. Huang, F. Ronning, E. D. Bauer, J. D. Thompson, M. A. Green, and R. J. Cava, *Phys. Rev. B* **79**, 012505 (2009).
 - ¹⁰ X. Zhu, F. Han, G. Mu, P. Cheng, B. Shen, B. Zeng, and H. H. Wen, *Phys. Rev. B* **79**, 220512(R) (2009).
 - ¹¹ N. Ni, J. M. Allred, B. C. Chan, and R. J. Cava, *Proc. Natl. Acad. Sci.* **108**, E1019 (2011).
 - ¹² I. I. Mazin, and M. D. Johannes, *Nat. Phys.* **5**, 141 (2009).
 - ¹³ K. Kuroki, S. Onari, R. Arita, H. Usui, Y. Tanaka, H. Kontani, and H. Aoki, *Phys. Rev. Lett.* **101**, 087004 (2008).
 - ¹⁴ Z. P. Yin, K. Haule, and G. Kotliar, *Nat. Phys.* **7**, 294 (2011).
 - ¹⁵ Q. Si, and E. Abrahams, *Phys. Rev. Lett.* **101**, 076401 (2008).
 - ¹⁶ J. X. Zhu, R. Yu, H. Wang, L. L. Zhao, M. D. Jones, J. Dai, E. Abrahams, E. Morosan, M. Fang, and Q. Si, *Phys. Rev. Lett.* **104**, 216405 (2010).
 - ¹⁷ N. Ni, S. Jia, Q. Huang, E. Climent-Pascual, and R. J. Cava, *Phys. Rev. B* **83**, 224403 (2011).
 - ¹⁸ C. Wang, M. Tan, C. Feng, Z. Ma, S. Jiang, Z. Xu, G. Cao, K. Matsubayashi, and Y. Uwatoko, *J. Am. Chem. Soc.* **132**, 7069 (2010).
 - ¹⁹ N. Ni, E. Climent-Pascual, S. Jia, Q. Huang, and R. J. Cava, *Phys. Rev. B* **82**, 214419 (2010).
 - ²⁰ J. B. He, D. M. Wang, H. L. Shi, H. X. Yang, J. Q. Li, and G. F. Chen, *Phys. Rev. B* **84**, 205212 (2011).
 - ²¹ J. Guo, S. Jin, G. Wang, S. Wang, K. Zhu, T. Zhou, M. He and X. Chen, *Phys. Rev. B* **82**, 180520(R) (2010).
 - ²² A. C. Larson, R. B. Von Dreele, general structure analysis system (GSAS), Los Alamos National Laboratory Report No. LAUR 86-748, (2000).
 - ²³ T. P. Perng, N. Kimizuka, and H. Steinfink, *J. Solid State Chem.* **40**, 92 (1981).
 - ²⁴ J. S. Swinnea, G. A. Eisman, T. P. Perng, N. Kimizuka, and H. Steinfink, *J. Solid State Chem.* **41**, 104 (1982).
 - ²⁵ H. Y. Hong, and H. Steinfink, *J. Solid State Chem.* **5**, 93 (1972).
 - ²⁶ B. Saparov, S. Calder, B. Sipos, H. Cao, S. Chi, D. J. Singh, A. D. Christianson, M. D. Lumsden, and A. S. Sefat, *Phys. Rev. B* **84**, 245132 (2011).
 - ²⁷ H. Lei, H. Ryu, A. I. Frenkel, C. Petrovic, *Phys. Rev. B* **84**, 214511 (2011).
 - ²⁸ H. Kabbour, E. Janod, B. Corraze, M. Danot, C. Lee, M. H. Whangbo, and L. Cario, *J. Am. Chem. Soc.* **130**, 8261 (2008).
 - ²⁹ E. Dagotto, *Rev. Mod. Phys.* **66**, 763 (1994).
 - ³⁰ M. Rotter, M. Tegel, D. Johrendt, I. Schellenberg, W. Hermes, and R. Pöttgen, *Phys. Rev. B* **78**, 020503(R) (2008).
 - ³¹ F. Han, X. Zhu, G. Mu, P. Cheng, and H. H. Wen, *Phys. Rev. B* **78**, 180503(R) (2008).
 - ³² G. M. Zhang, Y. H. Su, Z. Y. Lu, Z. Y. Weng, D. H. Lee, and T. Xiang, *EPL* **86**, 37006 (2009).
 - ³³ S. Y. Savrasov, *Phys. Rev. B* **54**, 16470 (1996).
 - ³⁴ X. Wan, Q. Yin, and S. Y. Savrasov, *Phys. Rev. Lett.* **97**, 266403 (2006).
 - ³⁵ X. Wan, J. Dong, and X. Dai, *Phys. Lett. A* **376**, 1759 (2012).
 - ³⁶ A. Kutepov, K. Haule, S. Y. Savrasov, and G. Kotliar, *Phys. Rev. B* **82**, 045105 (2010).
 - ³⁷ V. I. Anisimov, F. Aryasetiawan, and A. I. Lichtenstein, *J. Phys.: Condens. Matter* **9**, 767 (1997).
 - ³⁸ G. Kotliar, S. Y. Savrasov, K. Haule, and V. S. Oudovenko, *Rev. Mod. Phys.* **78**, 865 (2006).
 - ³⁹ M. J. Han, Q. Yin, W. E. Pickett, and S. Y. Savrasov, *Phys. Rev. Lett.* **102**, 107003 (2009).

⁴⁰ D. G. Free, and J. S. O. Evans, Phys. Rev. B **81**, 214433 (2010).